

H I ABSORPTION MEASUREMENTS TOWARD 15 PULSARS AND THE RADIAL
DISTRIBUTION OF DIFFUSE IONIZED GAS IN THE GALAXYD. A. FRAIL,^{1,2} J. M. CORDES,³ T. H. HANKINS,^{2,4} AND J. M. WEISBERG⁵*Received 1991 February 11; accepted 1991 May 24*

ABSTRACT

We report neutral hydrogen (H I) absorption measurements at 21 cm toward 15 pulsars with the Arecibo 305 m telescope and the VLA. The distances to these pulsars derived from the kinematic method have allowed us to rule out one potential pulsar-supernova remnant association while giving support to another. In addition, the secular change in the absorption spectrum toward one pulsar (PSR 1821+05) may provide independent confirmation of the recent discovery of AU-sized H I structures in the ISM.

A study of the radial distribution of the diffuse ionized medium has been carried out using mean electron density measurements made toward pulsars. With our new measurements and those from the literature, there are a total of 18 lines of sight that sample the electron density at small galactocentric radii. The data show a clear rise in the electron density in the inner Galaxy, to about 3 times the local average. From this and other evidence we argue that O stars are the principal heating agent of the warm ionized medium.

Subject headings: galaxies: The Galaxy — interstellar: matter — pulsars — radio sources: 21 cm radiation

1. INTRODUCTION

The existence of diffuse ionized gas outside discrete sources such as classical H II regions and planetary nebulae has been known for some time. However, only recently has it been widely recognized that this gas is an important constituent of the ISM. Its physical properties have been revealed by several independent diagnostics. These include pulse dispersion, low-frequency free-free absorption, radio and optical recombination lines, and optical forbidden lines. Despite the complications that arise when interpreting some of these measurements (e.g., radiative transfer effects, ionospheric blocking, extinction corrections, scattering, and limited sensitivity), they all paint a remarkably consistent picture of a well-distributed, ionized phase of the ISM with a density $n_e \simeq 0.2 \text{ cm}^{-3}$ and temperature $T_e \simeq 10^4 \text{ K}$ —the warm ionized medium (WIM; McKee & Ostriker 1977). Excellent reviews on this subject have been written by Kulkarni & Heiles (1988) and Reynolds (1984, 1989a).

Pulsars are one of the more useful probes of this diffuse ionized gas. The dispersion measure (DM, determined from multifrequency timing observations) is the column density of free electrons along the line of sight to a pulsar. If the distance D to a pulsar is known, then it is possible to make a simple and unambiguous determination of the mean free electron density along the line of sight to the pulsar.

$$\langle n_e \rangle = \frac{\int_0^D n_e(l) dl}{\int_0^D dl} = \frac{DM}{D} \text{ cm}^{-3}. \quad (1)$$

While much has been learned about the WIM, the key problem, which remains controversial, is the identity of the ionizing agent. The power requirement to maintain the level of

ionization that is observed is enormous, comparable to *all* the energy released by supernova remnants in our galaxy (Kulkarni & Heiles 1988). The primary purpose of this paper and a companion paper (Clifton et al. 1988, hereafter Paper I) was to make 21 cm absorption measurements toward high-DM pulsars, determine their distances using the kinematic method, and derive mean electron densities from equation (1). These observations are especially well suited to studying the electron density at low galactocentric radii and provide a crucial test for predictions of the principal heating agent for the WIM.

In this paper we present new 21 cm absorption and emission spectra toward 15 pulsars. In § 2 the techniques used to collect and reduce these data are discussed. In § 3 distances are derived to those pulsars to which the kinematic method can be successfully applied. Finally in § 4 these distance measurements are used together with those from the literature to investigate the radial distribution of the free electron density. The implications of our findings for identifying the heating source of the WIM are also discussed in § 4.

2. DATA ACQUISITION AND ANALYSIS

2.1. *Observational Techniques*

Determining $\langle n_e \rangle$ in equation (1) requires that both DM and D be known. While dispersion measures are a relatively simple observational parameter to obtain, pulsar distances are more difficult. The various pulsar distance determination methods have recently been reviewed by Frail & Weisberg (1990). The great majority of pulsar distances are obtained via the kinematic method, which was used both here and in Paper I. In brief, the neutral hydrogen (H I) emission and absorption spectra are measured toward the pulsar, and the features in these spectra are interpreted as lying in front of the pulsar (emission with absorption) or behind the pulsar (emission but no absorption). With the aid of a Galactic rotation curve these cloud velocities are converted to “kinematic” distances, yielding upper and lower limits on the pulsar distance.

There is a well-known problem of contamination from H I emission, which plagues single-dish absorption observations

¹ Department of Astronomy, University of Toronto.

² Postal address: National Radio Astronomy Observatory, Box 0, Socorro, NM 87801.

³ Astronomy Department, Space Sciences Building, Cornell University, Ithaca, NY 14853.

⁴ Department of Physics and Astronomy, NMIMT, Socorro, NM 87801.

⁵ Department of Physics and Astronomy, Carleton College, Northfield, MN 55057.

toward background continuum sources (see Colgan, Salpeter, & Terzian 1988, and references therein). Pulsars are near-ideal background sources for H I absorption measurement because their pulsed, periodic behavior can be used to correct for emission contamination in the beam *exactly*, without having to move off source. For more details on the technique of acquiring single-dish absorption spectra toward pulsars see Paper I.

Another solution to the emission problem is to exploit the spatial filter property of an interferometer. An interferometer with a given baseline is responsive only to angular structure on a scale inversely proportional to the baseline. H I emission is broadly distributed on angular scales from several degrees to a few arcminutes, while most background sources are smaller than this. More specifically, Crovisier & Dickey (1983) measured the spatial power spectrum of H I emission in a typical direction in the Galactic plane and found that it falls off as a power law with a slope between -2 and -3 , and that there is negligible power at baselines beyond 1000 to 2000 wavelengths. Thus, by choosing an interferometer with baselines in excess of these limits, but not large enough to resolve the background source, the absorption spectrum can be measured directly without the adverse effects from H I emission. The work of Dickey et al. (1983) and Garwood & Dickey (1989) are two recent examples where this particular method has been used with great success.

When using an interferometer, it is important to be able to have some means of acquiring data only during the interval that the pulsar is "ON" (i.e., has a nonzero flux). For the remaining time, the pulsar is "OFF," and if included this signal would add only noise to the final results. Thus by gating on the pulse the continuum flux density is enhanced over the period-averaged value by roughly f^{-1} . The signal to noise ratio (S/N) is also improved but by a factor $f^{-1/2}$, because we acquire data from only a fraction f of the total observing time. Since pulsars have small duty cycles (f) of order 2%–4% of their periods, the improvement can be substantial. For a typical pulsar with a duty cycle of about 4% we achieve a five fold improvement in S/N.

Pulsars are weak radio sources at L band. Consequently, in addition to special observing methods, large collecting areas are also required. In this regard the Arecibo 305-m⁶ and the Very Large Array⁷ (VLA) are the most sensitive telescopes available. On average the 305 m is 4 times more sensitive than the VLA, but this drops off rapidly toward its declination limits ($-2^\circ \leq \delta \leq +38^\circ$). The VLA is the only instrument capable of adequately studying the large numbers of high-DM pulsars within 34° of the Galactic center.

Two rather different experimental configurations were used to collect the data in this paper. The primary difference is that the VLA data acquisition hardware was explicitly synchronized with the pulsar period, while at Arecibo the synchronization was accomplished in software. Each of these systems will be discussed in turn, along with a description of the experimental setup, the data-taking process and the data reduction method.

2.2. The Arecibo 305 m Telescope Survey

The observations were made on two separate occasions: 1987 December 3–21 and 1988 February 4–15. The 21 cm dual

⁶ The Arecibo Observatory is part of National Astronomy and Ionosphere Center which is operated by Cornell University for the National Science Foundation.

⁷ The Very Large Array is operated by the National Radio Astronomy Observatory under contract with the National Science Foundation.

circularly polarized line feed was used with the low-noise FET receivers and the 3 level, 40 MHz autocorrelator. In all cases a bandwidth of 1.25 MHz was used. The number of lags or frequency channels was 256, except for PSR 1821+05 where it was 512. The technique used to acquire and analyze the data is identical to that described in Paper I and Frail (1989).

The first part of this survey was published in Paper I. Here we add seven new Arecibo observations, including a reobservation of PSR 1821+05. This brings the total number of Arecibo pulsar H I absorption observations made as part of this survey to 13.

2.3. The VLA Interferometer Survey

The VLA observations were made from 1987 December to 1989 May. At all times the observing bandwidth was 3.125 MHz, and the number of frequency channels was 256. Only the central 128 channels or 1.5625 MHz of data were written to tape. The VLA was used in the A-, A/B-, B/C-, and C-configurations. For the last two of these array configurations some H I emission structure was seen in the low uv spacings. Data from 0 to 1.4 $k\lambda$ were therefore excluded in making the spectra.

At the VLA the 21 cm absorption spectrum toward a pulsar is obtained by operating the array in the "phased array" mode, where the delays of each antenna are adjusted so that a pencil beam is formed. The array is first pointed at a strong point source with a well-known position within 15° of the pulsar. An on-line program solves for the peculiar phases for each antenna and adjusts the interferometer delay lines so that the relative phases with respect to some reference antenna near the center of the array are equal (Dickey et al. 1983). The antenna phases obtained this way are stable over periods between 30 minutes to a few hours. The array is then pointed at a pulsar with the phases compensated for. The (now coherent) signals from each antenna are then added together resulting in a pencil beam in the direction of the pulsar.

The coherent sum is square-law detected and passed to a dual-processor Intel 286-based data acquisition system built at Dartmouth College by T. H. Hankins and E. Horton. This system forms a synchronous average pulsar pulse profile by sampling at the continuously updated Doppler-corrected pulsar period. It also generates a synchronous pulsed logic gating signal which we align with the pulsar pulse. Once aligned, this signal is used to gate the VLA correlator.

In this gate mode, the VLA correlator then computes cross-correlation functions (CCFs) between antenna pairs only during the ON-pulse interval. These CCFs are accumulated in correlator memory for some fixed integration period (usually 10 s). They are then passed to an array processor where the correlator bias is removed, and a discrete Fourier transform is performed, producing uncalibrated cross power spectra (visibility data) which are then written to tape.

In calibrating the data we followed standard VLA procedures. For all pulsars but 0329+54, the primary flux calibrator was 3C 286. In order to use 3C 286 also as a bandpass calibrator, uncontaminated by H I emission or absorption, we moved 150 km s^{-1} above and below the center velocity and averaged the two resulting spectra. The same procedure was followed with 0329+54 except that 3C 48 was used instead of 3C 286. As noted by Dickey et al. (1983) the full synthesis imaging capability of the VLA is not required for point source spectroscopy. Recognizing that the Fourier transform of a delta function is a constant, it follows that the final absorption

TABLE 1
PARAMETERS FOR ARECIBO OBSERVATIONS

Pulsar (1)	Right Ascension (2)	Declination (3)	Δt (minutes) (4)	δV (km s^{-1}) (5)	σ_r (6)
1821+05.....	18 ^h 21 ^m 4 ^s 0	05°48'47"	180	0.62	0.08
1900+05.....	19 00 15.5	05 52 01	460	3.09	0.03
1900+06.....	19 00 20.0	06 11 25	620	2.06	0.06
1913+10.....	19 13 7.6	10 04 25	340	3.09	0.04
1929+20.....	19 29 57.2	20 14 18	450	2.06	0.06
1930+22.....	19 30 12.5	22 15 19	550	4.12	0.06
2035+36.....	20 35 31.8	36 10 51	480	3.09	0.07

spectrum is formed by calculating a vector sum of all the visibility data separately for each velocity channel.

The VLA, as an interferometer, is essentially insensitive to the broadly distributed H I emission. As a result the NRAO 140 ft telescope was used in 1990 August to obtain emission spectra toward each of our pulsars except PSR 1641–45, which is below the elevation limits for the telescope. The dual circularly polarized feeds were used with the HEMP receivers whose cold sky temperatures are approximately 18 K. Both polarizations were recorded, with 512 frequency channels each for a full bandwidth of 2.5 MHz, or a channel resolution of 1.03 km s^{-1} . Data reduction was performed in the NRAO POPS package. Following Burton (1985), the spectra have been converted to brightness temperature by multiplying the original data (in antenna temperature) by 1.35.

3. RESULTS

Figures 1 to 7 shows the H I absorption and emission profiles toward each of the pulsars observed with the Arecibo 305 m telescope. Also indicated is the velocity-distance relation deduced by assuming a Fich, Blitz, & Stark (1989) flat rotation curve for the Galaxy with IAU 1985 constants (i.e., $R_0 = 8.5$ kpc, $\theta_0 = 220 \text{ km s}^{-1}$). Figures 8 to 15 are nearly identical to Figures 1 to 7 except that they are for pulsars observed at the VLA. Unless otherwise stated we will use IAU 1985 constants and the Fich et al. (1989) flat rotation curve throughout. Damour & Taylor (1991) give a simple equation for rescaling distances using different values of these constants, valid in the case of a linear rotation curve. The distance scales linearly with the value of R_0 , while for θ_0 the dependence is weaker.

Table 1 contains details relevant to the interpretation of Figures 1–7. The right ascension and declination values in columns (2) and (3) are the ones used during the observations.

The total observing time on source is given as Δt in column (4). The channel separation is either 1.03 km s^{-1} (4.88 kHz) or 0.52 km s^{-1} (2.44 kHz), depending on whether 256 or 512 channels were used across the 1.25 MHz band. Some of the absorption spectra needed Hanning smoothing. The final velocity resolution δV for each of the absorption spectra is listed in column (5). The velocity resolution is defined as the width at half-power. For all of the emission spectra and a few of the absorption spectra no smoothing was done. In these cases the velocity resolution is simply 1.2 times the channel spacing. Column (6) contains the 1σ noise level in the absorption spectrum, estimated over a region free of any absorption features.

Table 2 contains details relevant to the interpretation of Figures 8–15. The columns are the same as those in Table 1. For all absorption observations the channel separation was 12.2 kHz (2.57 km s^{-1}). Some of the spectra required Hanning smoothing. The spectra for the pulsars 1830–08 and 1844–04 are not shown because of inadequate signal-to-noise.

In interpreting these spectra we closely followed the kinematic method as outlined by Frail & Weisberg (1990). The basic method is to use the absorption and emission spectra toward the pulsar to determine upper and lower velocity limits (V_U and V_L), and to derive distance limits (D_L and D_U) using these velocities and a galactic rotation curve. We departed slightly from the convention of previous pulsar distance assignments (e.g., Paper I) in that our distances are derived from the velocity limit directly. We do not shift our velocities to allow for (typical) errors of $\pm 7 \text{ km s}^{-1}$. These errors are instead reflected in an uncertainty assigned to each distance estimate.

In the following two subsections each pulsar and its spectra are considered in turn and an explanation is given to how and why we arrived (or failed to arrive) at our final distance estimate(s). A summary of our derived parameters along with

TABLE 2
PARAMETERS FOR VLA OBSERVATIONS

Pulsar (1)	Right Ascension (2)	Declination (3)	Δt (minutes) (4)	δV (km s^{-1}) (5)	σ_r (6)
0329+54.....	03 ^h 29 ^m 11 ^s 06	54°24'37".6	38	3.09	0.04
1556–44.....	15 56 11.02	–44 30 16.7	134	3.09	0.04
1641–45.....	16 41 10.36	–45 53 36.7	18	3.09	0.02
1800–21.....	18 00 51.1	–21 37 18	432	5.15	0.09
1804–08.....	18 04 53.91	–08 48 10.7	162	3.09	0.12
1829–08.....	18 29 53.40	–08 29 19.6	408	5.15	0.06
1830–08.....	18 30 56.68	–08 29 51.6	234
1844–04.....	18 44 44.41	–04 05 34.4	174
1911–04.....	19 11 15.16	–04 46 0.0	246	3.09	0.07
2255+58.....	22 55 54.2	58 53 10	138	5.15	0.08

TABLE 3
 DERIVED PARAMETERS

Pulsar (1)	l (2)	b (3)	DM (pc cm^{-3}) (4)	V_L (km s^{-1}) (5)	V_U (km s^{-1}) (6)	D_L (kpc) (7)	D_U (kpc) (8)	Electron Density (cm^{-3}) (9)
0329+54.....	145.0	-1.2	26.8	-31	-35	1.7 ± 0.7	2.0 ± 0.8	$0.013 \leq \langle n_e \rangle \leq 0.016$
1641-45.....	339.2	-0.2	475	-59	-77	4.2 ± 0.3	5.0 ± 0.2	$0.095 \leq \langle n_e \rangle \leq 0.11$
1800-21.....	8.4	0.1	234.2	+27	+40	4.0 ± 0.6	4.9 ± 0.3	$0.048 \leq \langle n_e \rangle \leq 0.059$
1804-08.....	20.1	5.6	112.8	+14	...	1.5 ± 0.7	...	$\langle n_e \rangle \leq 0.075$
1821+05.....	35.0	8.9	67.5	+20	...	1.6 ± 0.5	...	$\langle n_e \rangle \leq 0.042$
1829-08.....	23.3	0.3	300	+73	+100	4.7 ± 0.3	5.8 ± 0.3	$0.052 \leq \langle n_e \rangle \leq 0.064$
1900+05.....	39.5	0.2	179.7	+44	+61	3.1 ± 0.4	4.3 ± 0.5	$0.042 \leq \langle n_e \rangle \leq 0.058$
1900+06.....	39.9	0.4	530 ± 25	TP	-30	6.5 ± 1.4	15.8 ± 0.8	$0.034 \leq \langle n_e \rangle \leq 0.082$
1913+10.....	44.7	-0.7	246.1	TP	-29	6.0 ± 1.5	14.5 ± 0.8	$0.017 \leq \langle n_e \rangle \leq 0.041$
1929+20.....	55.6	0.6	211.0	TP	-57	4.8 ± 1.8	14.9 ± 0.9	$0.014 \leq \langle n_e \rangle \leq 0.044$
1930+22.....	57.4	1.6	211.3	-16	-50	10.4 ± 0.6	13.7 ± 0.7	$0.015 \leq \langle n_e \rangle \leq 0.020$
2255+58.....	108.8	-0.6	151.1	-53	...	3.3 ± 0.7	...	$\langle n_e \rangle \leq 0.046$

other useful information is given in Table 3. Columns (2) and (3) list the galactic coordinates for each pulsar, while column (4) has the dispersion measure. An uncertainty in the DM is quoted only when it exceeds 2%. The velocity and distance limits are given in columns (5)–(8). The electron density in column (9) is calculated using equation (1).

3.1. Arecibo Results

3.1.1. PSR 1821+05: (l, b) = ($35^\circ 0, 8^\circ 9$), DM = $67.5 \text{ cm}^{-3} \text{ pc}$

Clifton et al. (1988) observed this pulsar in 1987 February and noted a deep, unresolved absorption component at +6–7

km s^{-1} . The velocity resolution was increased from 1.2 km s^{-1} to the present 0.6 km s^{-1} in order to follow up on the study of this unusual feature. The deep feature is no longer visible in this new spectrum. In its place is a weaker ($\tau = 1$), more resolved feature. The new spectrum more closely resembles an earlier, noisier spectrum toward PSR 1821+05 made by Weisberg, Rankin, & Boriakoff (1987). The change in the spectrum over a period of approximately 1 yr suggests either that the deep feature was spurious or, more interestingly, that it was seen because of the relative motion of the pulsar and the diffuse H I. Clifton et al. discounted a spurious origin as they noted that the deep feature was visible in individual high signal-to-noise spectra over the entire 3 week observing period. Comparing the H I profiles we see that there has been a change in the column density of order 10^{20} cm^{-2} .

Using the interstellar scintillation technique Cordes (1986) has determined the space velocity of this pulsar to be 19 km

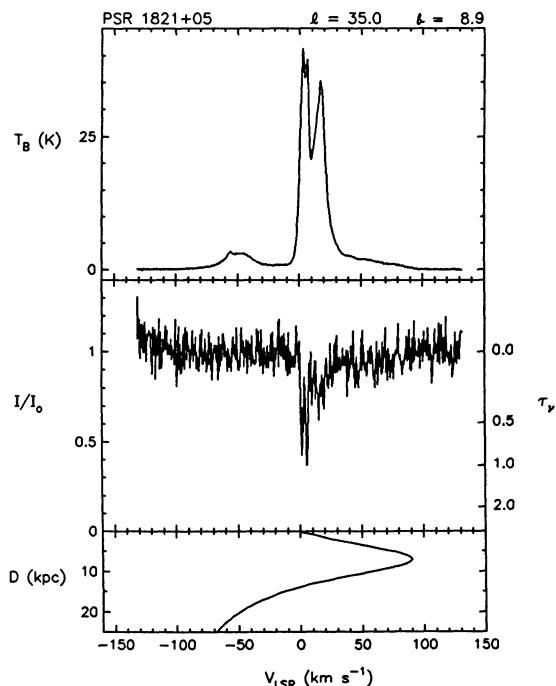


FIG. 1.—Neutral hydrogen spectra toward pulsars made with the Arecibo 305 m telescope. Pulsar name is given in the upper left corner of each plot, while Galactic coordinates are in the upper right. Upper portion of each panel shows the H I emission spectrum toward the pulsar. Brightness temperatures have been converted from antenna temperatures using the Weaver & Williams (1974) survey. Central portion of each panel shows the absorption spectrum toward the pulsar, while the lower portion shows a Fich et al. (1987) flat rotation curve for the conversion of radial velocities to distances.

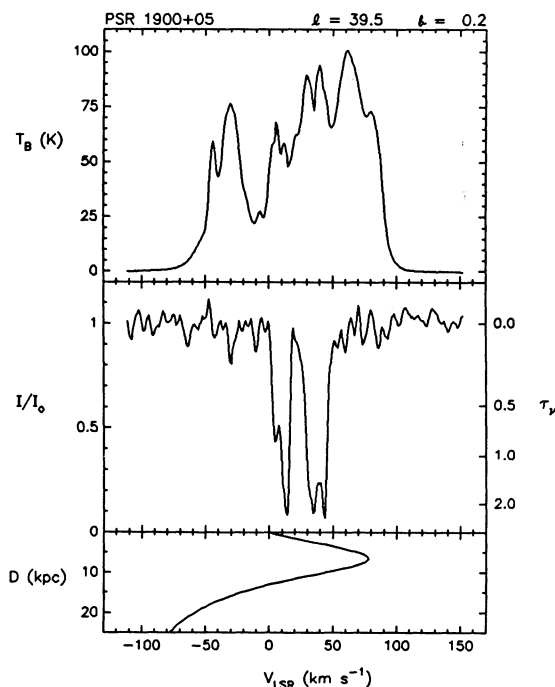


FIG. 2.—As in Fig. 1

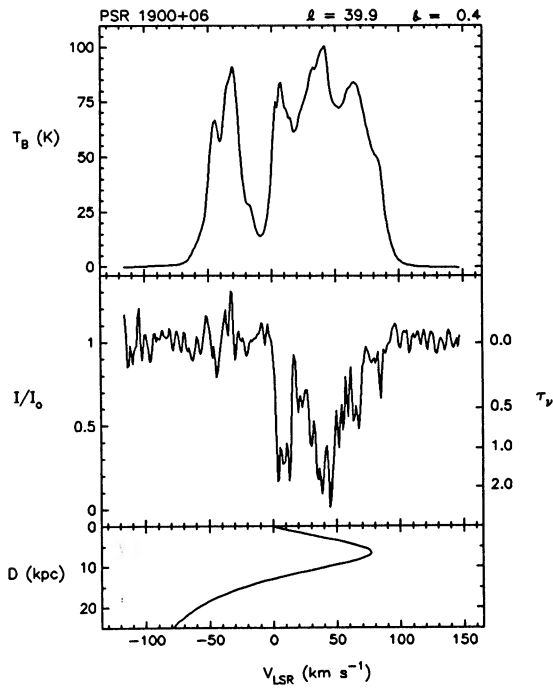


FIG. 3.—As in Fig. 1

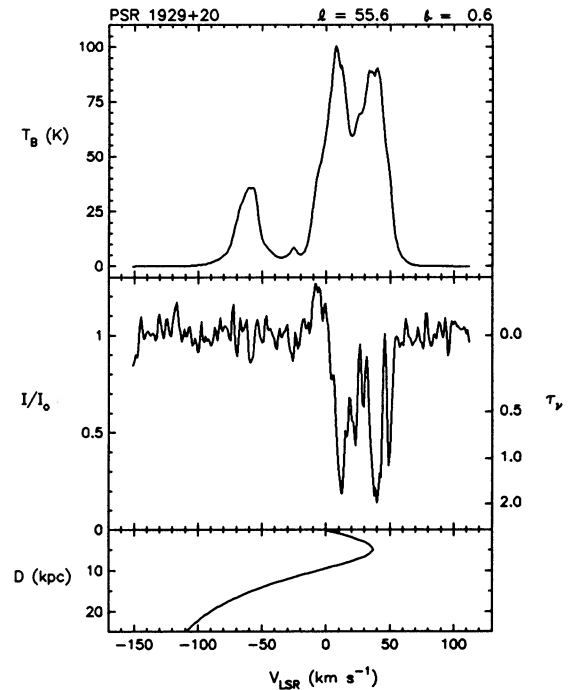


FIG. 5.—As in Fig. 1

s^{-1} or 4 AU yr^{-1} . If the secular change in the absorption spectrum toward PSR 1821+05 is real, then it is an independent confirmation of the recent discovery of AU-sized H I structures seen against bright continuum sources at VLBI resolutions (Diamond et al. 1989). The existence of small-scale structures in the ISM has important implications and needs further study.

The farthest detectable line in our spectrum is at $+20 \text{ km s}^{-1}$. This is similar to the value of $+18.6 \text{ km s}^{-1}$ derived from

the Clifton et al. (1988) spectrum. We therefore derive a lower distance limit of 1.6 kpc to the pulsar. No upper distance limit is possible in this direction.

3.1.2. PSR 1900+05: $(l, b) = (39^\circ.5, 0^\circ.2)$, $DM = 179.7 \text{ cm}^{-3} \text{ pc}$

Strong H I emission extends throughout the allowable velocity range, whereas deep H I absorption is visible only from 0 to $+44 \text{ km s}^{-1}$. The latter velocity is chosen as the lower limit, corresponding to a distance of 3.1 kpc. The nearest emission

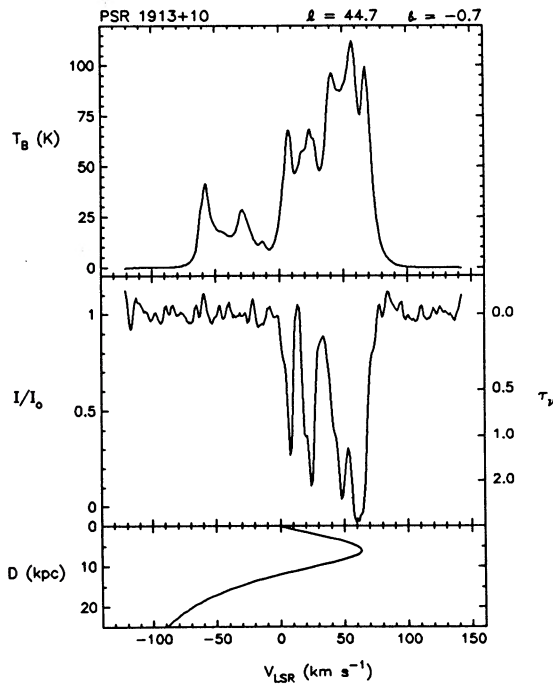


FIG. 4.—As in Fig. 1

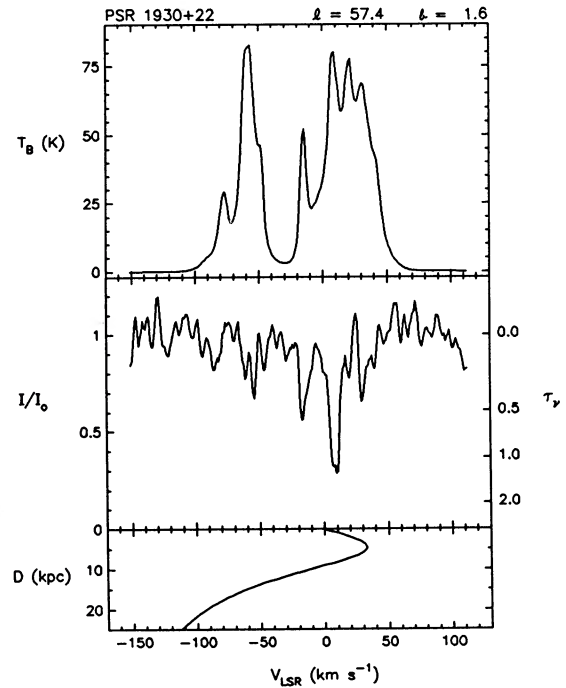


FIG. 6.—As in Fig. 1

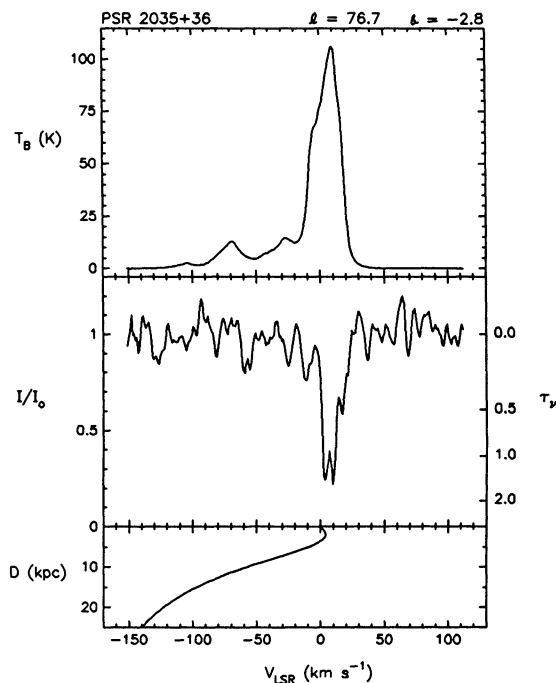


FIG. 7.—As in Fig. 1

peak beyond this is at $+61 \text{ km s}^{-1}$ and has a brightness temperature of 100 K. We choose this feature as our upper velocity limit, for which we derive an upper distance of 4.3 kpc to the pulsar.

3.1.3. PSR 1900+06: (l, b) = ($39^{\circ}9, 0^{\circ}4$), $DM = 530 \text{ cm}^{-3} \text{ pc}$

In this spectrum we do not see evidence for absorption at negative velocities. We therefore take -30 km s^{-1} , the velocity of an H I emission peak, as a hard upper limit on which to calculate the distance to the pulsar. The higher noise level around -30 km s^{-1} is the result of the strong emission at these velocities.

Absorption in the spectrum of PSR 1900+06 extends beyond the $+44 \text{ km s}^{-1}$ limit of PSR 1900+05 and right up to the tangent point. However, the tangent point absorption is not typical of what is seen in this general direction. The optical depth of individual features steadily decreases from $\tau = 2.0$ at $+45 \text{ km s}^{-1}$ to $\tau = 0.4$ at the tangent point velocity ($\sim +85 \text{ km s}^{-1}$). In addition there is a gap of almost 20 km s^{-1} , centered on $+75 \text{ km s}^{-1}$, for which no absorption can be detected. This suggests one of two things. Either the pulsar is not significantly beyond the tangent point (and possibly closer than the far-side distance corresponding to $+75 \text{ km s}^{-1}$), or there is a paucity of cold material in this direction. Support for the former explanation comes from studying the absorption spectra of nearby sources. For example, the spectra toward G37.7+0.1 (Silvergate & Terzian 1978), G39.6+0.0 (Garwood & Dickey 1989), and W49A at (l, b) = $43^{\circ}2, 0^{\circ}0$ (Dickey & Benson 1982) all show substantial absorption ($\tau > 1$) at their tangent points. However, this evidence should not be taken as conclusive, because all of these sources are closer to the Galactic plane than 1900+06.

In summary, for 1900+06 we choose the tangent point as the lower limit and take the upper limit to be -30 km s^{-1} , recognizing that the pulsar could well be much closer than the

upper limit. From these velocity limits we derive distance limits of 6.5–15.8 kpc for this pulsar.

3.1.4. PSR 1913+10: (l, b) = ($44^{\circ}7, -0^{\circ}7$), $DM = 246.1 \text{ cm}^{-3} \text{ pc}$

Strong absorption and emission is clearly visible at positive velocities up to the tangent point. The deep absorption at the tangent point is chosen as the lower limit. There is no evidence of absorption at negative velocities despite the low noise level in the absorption spectra and bright emission at -29 km s^{-1} ($T_b \approx 28 \text{ K}$) and -57 km s^{-1} ($T_b \approx 42 \text{ K}$). We assign the upper limit to the -29 km s^{-1} emission feature. On the basis of these velocity limits we derive lower and upper distance limits of 6.0 and 14.5 kpc, respectively.

3.1.5. PSR 1929+20: (l, b) = ($55^{\circ}6, 0^{\circ}6$), $DM = 211.0 \text{ cm}^{-3} \text{ pc}$

Deep absorption is visible extending from 0 km s^{-1} out to the tangent point but not beyond this to negative velocities. On this basis, we assign the tangent point to be the lower limit. There is a bright emission feature ($T_b \approx 36 \text{ K}$) at -57 km s^{-1} which we take as the upper limit. From these velocity limits we derive distance limits of 4.8–14.9 kpc. Reich et al. (1986) note that this pulsar lies near the center of an extended radio source which they conclude is an H II region. No distance information is available for the H II region.

3.1.6. PSR 1930+22: (l, b) = ($57^{\circ}4, 1^{\circ}6$), $DM = 211.3 \text{ cm}^{-3} \text{ pc}$

This was the weakest pulsar of those we observed, and so its absorption spectrum has a high noise level. Only two positive detections of absorption lines were made, one at $+9 \text{ km s}^{-1}$ and another at -16 km s^{-1} . Several additional features at both positive and negative velocities are below our 3σ criterion imposed for the detection of “real” features.

It would appear that there is very little cold gas at the tangent point distance in this direction. Absorption spectra obtained toward a nearby point source 1923+210 at (l, b) = ($55^{\circ}6, 2^{\circ}3$) by Dickey et al. (1983) and Colgan et al. (1988) evidently confirm this conclusion. The strongest absorption line in the spectrum toward 1923+210 is at $+10 \text{ km s}^{-1}$. There are several absorption lines at velocities leading up to the tangent point, but these are rather weak ($\tau < 0.2$).

At negative velocities in the spectrum of 1923+210 there are several discrete absorption lines from -45 to -85 km s^{-1} , but there is no absorption (or centrally peaked emission) at -16 km s^{-1} as is seen for 1930+22. In the H I latitude-velocity plots of Weaver & Williams (1974) there is an isolated emission feature at this velocity that is seen to have a very narrow extent in latitude but can be followed over 3° in longitude, centered on $l = 57^{\circ}$. We take this velocity as the lower limit for 1930+22. However, we cannot rule out that this feature might be local, but with a very high random velocity relative to the l_{sr} . The upper limit is indicated at -50 km s^{-1} , the velocity of a bright, narrow feature in the emission spectrum in this direction with no corresponding absorption. The extra noise in the absorption spectrum at this velocity is due to the strong emission feature.

On the basis of these velocity limits we derive distance limits of 10.4–13.7 kpc. Routledge & Vaneldik (1988) discovered a supernova remnant (SNR) at 1420 and 408 MHz with a $1^{\circ}7$ diameter that surrounds PSR 1930+22. They derive a distance of 4.5 kpc to the SNR based on the well-known radio surface brightness–diameter relation and argue that the dispersion measure distance to the pulsar favors a real physical association between the two objects. Kovalenko (1989) has observed the SNR at 102.5 MHz and derives a closer distance of 2.3 kpc

from the same considerations. In either case our new measurements place the pulsar at a distance that is well beyond that of the SNR, and we conclude that the association is only a line-of-sight coincidence.

3.1.7. 2035+36: $(l, b) = (76.7, -2.8)$, $DM = 92 \text{ cm}^{-3} \text{ pc}$

The absorption spectrum is noisy, but it is clear that absorption can be detected out to the tangent point. However, there is a large amount of velocity crowding in this direction, and this makes determining kinematic distances difficult. In fact, the emission and absorption extend out beyond velocities allowed by pure circular rotation. At -12 km s^{-1} there is an absorption feature at $\tau = 0.3$, that is just below the 3σ noise level. We feel that this feature is probably spurious. The feature does not coincide with a nearby local peak in the H I emission near -5 km s^{-1} . This is in contrast to the absorption in the spectra of several nearby point sources including 2023+335 at $(l, b) = (73.1, -2.4)$ by Dickey et al. (1983).

We cannot assign either a reliable upper or lower limit, and therefore we are unable to derive a distance to this pulsar.

3.2. VLA Results

Figures 8 to 15 show the H I absorption profiles toward most of the pulsars observed with the VLA.

3.2.1. PSR 0329+54: $(l, b) = (145.0, -1.2)$, $DM = 26.8 \text{ cm}^{-3} \text{ pc}$

There is close agreement between our spectrum and those of Gordon, Gordon, & Shalloway (1969), Gordon & Gordon (1973), and Booth & Lyne (1976). We agree with the latter authors' choice of a weak absorption feature at -31 km s^{-1} as the lower velocity limit. No absorption can be detected beyond this, so the position of a bright emission peak ($T_b > 70 \text{ K}$) in the Perseus arm at -35 km s^{-1} is assigned as the upper limit.

The source 3C 86 lies only 1° away at $(l, b) = (143.9, -1.1)$. In contrast with PSR 0329+54, the spectrum of 3C 86 by

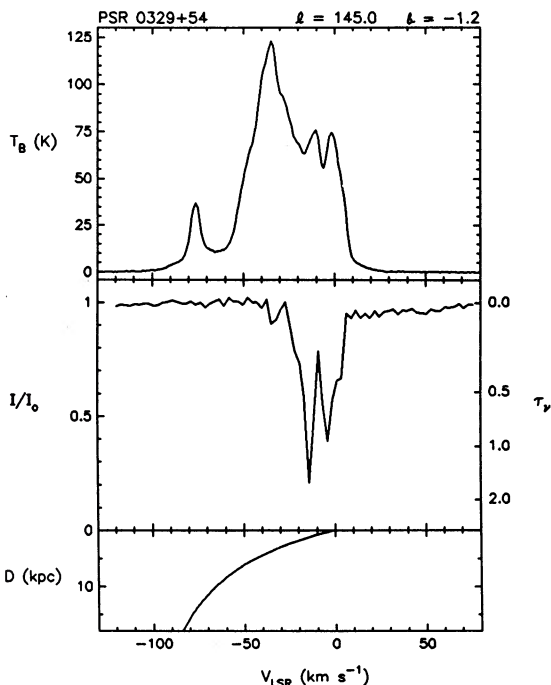


FIG. 8.—Neutral hydrogen absorption spectra toward pulsars made with the VLA. (For details see previous figure caption.)

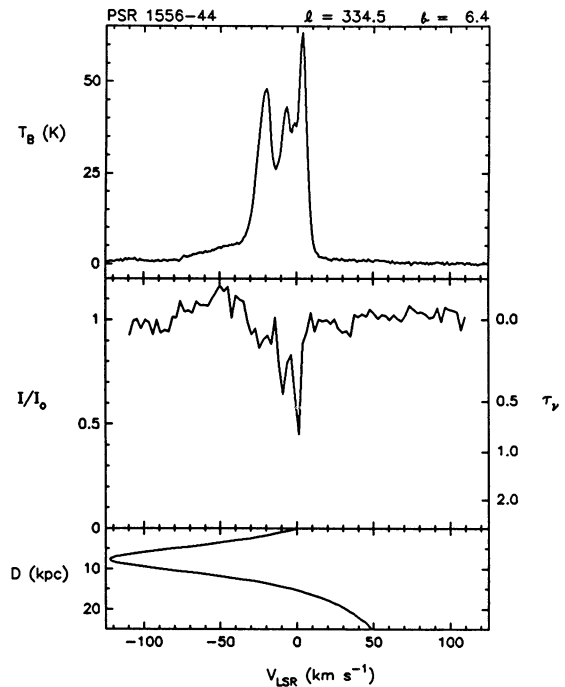


FIG. 9.—As in Fig. 8

Dickey et al. (1983) shows deep absorption at -35 km s^{-1} . This provides strong confirmation of our choice of the upper velocity limit.

The Perseus arm in this direction has known systematic deviations from pure circular rotation (Roberts 1972). Here again we follow the approach taken by Frail & Weisberg (1990), decreasing the velocity by a factor of 1.6 before calculating the distance from the Fich et al. (1989) rotation curve. This leads to lower and upper distance limits of 1.7 and 2.0 kpc, respectively, placing the pulsar near the inner edge of the Perseus arm (Roberts 1972; Gerasimenko 1983). This result is not far from Gordon & Gordon's limit of 1.3–2.0 kpc, but quite different from Booth and Lyne's $2.6 \pm 0.3 \text{ kpc}$. The first authors tried to account for noncircular Perseus arm motions, while the latter authors used the Schmidt (1965) galactic rotation model directly.

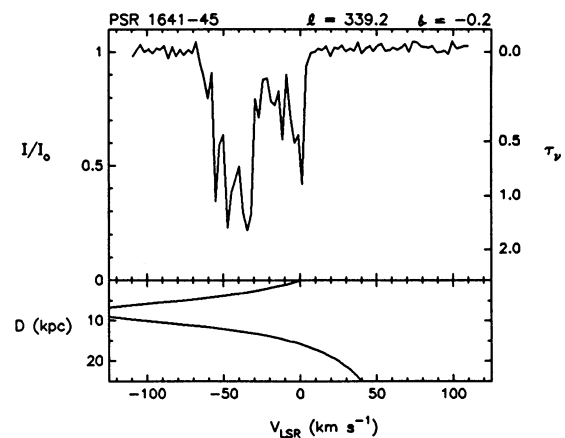


FIG. 10.—As in Fig. 8

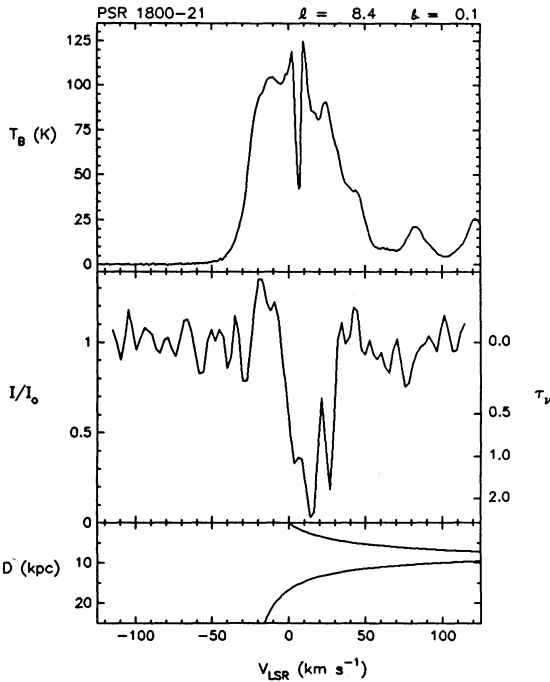


FIG. 11.—As in Fig. 8

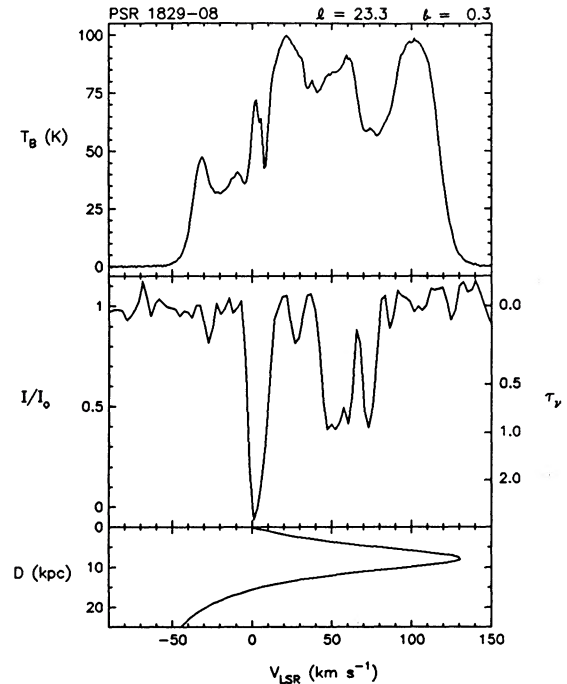


FIG. 13.—As in Fig. 8

3.2.2. PSR 1556-44: $(l, b) = (334^\circ.5, 6^\circ.4)$, $DM = 58.8 \text{ cm}^{-3} \text{ pc}$

Unfortunately, it appears that interstellar scintillation or low-level H I emission fluctuations have distorted the frequency structure of this spectrum. Consequently absorption can be positively identified only at two velocities, $+2$ and -9 km s^{-1} . These are likely local absorption features to which no kinematic distance can be assigned. The last emission peak in this direction occurs just beyond -20 km s^{-1} , but here the

distortion in the baseline is large. We assign neither an upper nor a lower limit for these reasons.

3.2.3. PSR 1641-45: $(l, b) = (339^\circ.2, -0^\circ.2)$, $DM = 475 \text{ cm}^{-3} \text{ pc}$

Ables & Manchester (1976) have previously observed this pulsar and derived its distance. We agree with these authors that the -59 km s^{-1} feature is the most distant absorption feature that can be detected. We assign this to be our lower

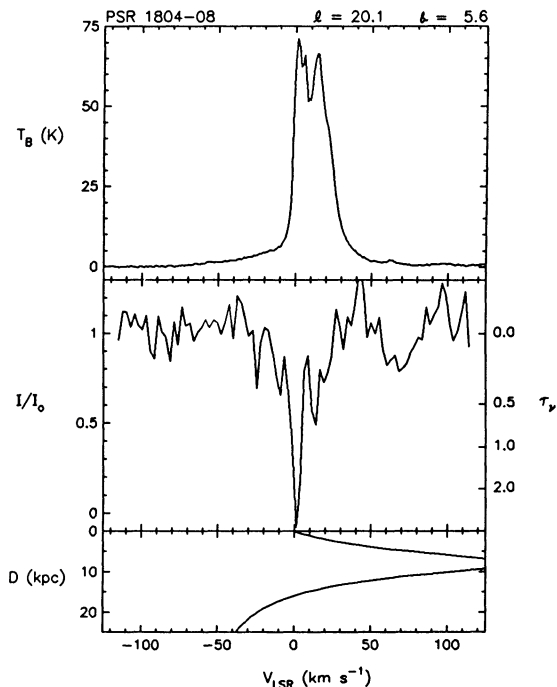


FIG. 12.—As in Fig. 8

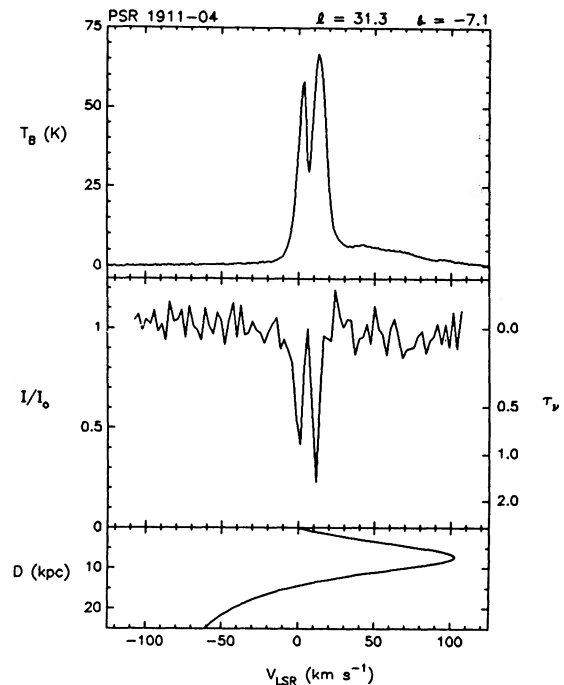


FIG. 14.—As in Fig. 8

limit and the strong feature seen in Ables & Manchester's emission spectrum at -77 km s^{-1} as the upper limit. On the basis of these velocity limits we derive lower and upper distance limits of 4.2 and 5.0 kpc, respectively.

3.2.4. *PSR 1800-21*: $(l, b) = (8^\circ.4, 0^\circ.1)$, $DM = 234.2 \text{ cm}^{-3} \text{ pc}$

The most distant absorption feature at $+27 \text{ km s}^{-1}$ fixes the lower limit. The emission spectrum in this direction shows a secondary peak at $+40 \text{ km s}^{-1}$ with $T_b \simeq 40 \text{ K}$. Since there is no detectable absorption at this velocity, we assign our upper limit at $+40 \text{ km s}^{-1}$. There may be some emission contamination of the absorption spectrum, notably at -20 km s^{-1} , near the peak of a broad emission feature in this direction.

The absorption spectra of several nearby sources add support to our choice of these limits. They include G7.5+0.1 (Garwood & Dickey 1989), G10.1+0.7 (Gathier, Pottasch, & Goss 1986), and W31 at $(l, b) = (10^\circ.2, -0^\circ.3)$ (Kalberla, Goss, & Wilson 1982). All of these spectra have absorption extending to velocities beyond $+40 \text{ km s}^{-1}$.

On the basis of these velocity limits we derive lower and upper distance limits of 4.0 and 4.9 kpc, respectively. Kassim & Weiler (1990) have discussed the possibility of an association of this pulsar with the W30 SNR. They drive a distance of $5.5 \pm 1 \text{ kpc}$ to the SNR based on distances to foreground and background H II regions. Our pulsar distance measurement would seem to support their claim.

3.2.5. *PSR 1804-08*: $(l, b) = (20^\circ.1, 5^\circ.6)$, $DM = 112.8 \text{ cm}^{-3} \text{ pc}$

The absorption spectrum is noisy and difficult to interpret. There are four features that exceed the 3σ noise level. These are at -25 , -9 , $+1$, and $+14 \text{ km s}^{-1}$. If real, the negative velocity features would put the pulsar several kpc above the Galactic plane. However, they are of the same magnitude as several noise features near $+50$ and $+100 \text{ km s}^{-1}$. We consider these to be spurious and set a lower limit of $+14 \text{ km s}^{-1}$ where $T_b = 66 \text{ K}$. Beyond this velocity the H I emission is weak, and we are therefore not able to assign an upper velocity limit.

The lower distance limit corresponding to this velocity is 1.5 kpc.

3.2.6. *PSR 1829-08*: $(l, b) = (23^\circ.3, 0^\circ.3)$, $DM = 300.0 \text{ cm}^{-3} \text{ pc}$

Absorption is visible at positive velocities with the most distant feature at $+73 \text{ km s}^{-1}$. We assign this as the lower limit. The tangent point could be considered a hard upper limit, but we note that the emission in this direction peaks at a lower velocity of $+100 \text{ km s}^{-1}$. This is taken as the upper velocity limit.

There are several useful comparison sources in the vicinity. NRAO 572 at $(l, b) = (25^\circ.4, -0^\circ.2)$ and G24.8+0.1, for example, have been observed in the H I line by Dickey & Benson (1982) and Caswell et al. (1975), respectively. Both sources show prominent emission and absorption at positive velocities out to about $+100 \text{ km s}^{-1}$. We also note that an absorption spectrum toward G24.0+0.2 obtained by Garwood & Dickey (1989) is nearly identical to that of the pulsar, only $0^\circ.7$ away.

On the basis of these velocity limits we derive lower and upper distance limits of 4.7 and 5.8 kpc, respectively. On radio surveys of this area the pulsar is positionally coincident with a $7' \times 9'$ region of extended emission (e.g., Altenhoff et al. 1979). Lockman's (1989) recombination line survey detected H125 α and H127 α at $+108.8 \text{ km s}^{-1}$ in this direction, so the emission is likely due to a background H II region.

3.2.7. *PSR 1911-04*: $(l, b) = (31^\circ.3, -7^\circ.1)$, $DM = 89.4 \text{ cm}^{-3} \text{ pc}$

The absorption spectrum toward this pulsar has components at $+1$ and $+11 \text{ km s}^{-1}$. We cannot assign a kinematic distance to this pulsar based on these (presumably) local features. The H I emission drops to a low level at more positive velocities, so it is of little help in assigning an upper limit.

3.2.8. *2255+58*: $(l, b) = (108^\circ.8, -0^\circ.6)$, $DM = 151.1 \text{ cm}^{-3} \text{ pc}$

There are two absorption features in the spectrum, each coincident with peaks of H I emission in this direction. The last absorption feature is at -53 km s^{-1} , and this we assign as the lower limit. Beyond this velocity the brightness temperature of the H I emission drops quickly, so we are unable to derive an upper limit.

After correcting for noncircular motions (see PSR 0329+54) the lower distance limit becomes 3.3 kpc. The inner edge of the Perseus arm in this direction is placed at about 2.8 kpc by Roberts (1972) and Gerasimenko (1983). Therefore, PSR 2255+58 is either within or beyond the Perseus arm.

4. DISCUSSION

4.1. The Galactic Radial Dependence of n_e

4.1.1. Comparison with Previous Work

Because of the paucity of direct measurements of $\langle n_e \rangle$ in the inner Galaxy, previous investigators have used indirect methods for determining the electron density distribution. These methods usually involve a statistical study of some property of the pulsar population, subject to a plausible constraint. This in turn imposes a limitation on the allowable range that the electron density can take.

For example, Lyne, Manchester, & Taylor (1985, hereafter LMT) derived the radial term in their model by applying a correction factor so that the scale height of the pulsars in their sample remained independent of the galactocentric radius R . The volume-averaged electron density in the LMT model is given as

$$n_e(R, z) \equiv \bar{n}_e(R, z) \bar{f}(R, z) \\ = \left[0.025 + 0.015 \exp\left(-\frac{|z|}{70}\right) \right] \left[\frac{2.0}{1 + R/R_o} \right] \text{ cm}^{-3}, \quad (2)$$

where z is the distance above the Galactic plane (in parsecs) and R_o is the Sun's distance from the Galactic center, and \bar{n}_e and \bar{f} are values for the density and filling factor of the ionized gas at a given point (R, z) in the Galaxy. While the LMT model is the most recent and best determined, similar work has been carried out by other groups (Gómez-González & Guélin 1974; del Romero & Gómez-González 1981; Vivekanand & Narayan 1982; Harding & Harding 1982).

All these indirect approaches have indicated that the electron density must rise in the inner Galaxy, but the degree to which the density is enhanced in this region over its local value is not well known. The problem is that the number of pulsars at small galactocentric radii is insufficient to accurately constrain the electron density through statistical means. With the completion of the observations reported in § 3 there are now 18 pulsars in the "inner Galaxy" ($|l| \leq 45^\circ$, $|b| \leq 2^\circ$ and $DM \geq 100 \text{ pc cm}^{-3}$) toward which *direct* measurements of $\langle n_e \rangle$ have been made. Table 4 lists the additional pulsars from the literature (Frail & Weisberg 1990; Lyne et al. 1990) that meet these criteria in a format similar to Table 3. The data in Tables 3 and 4 more than double the number available when

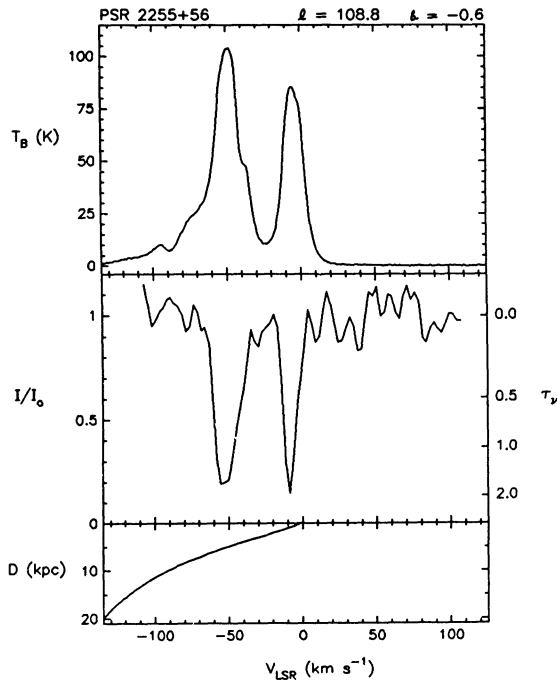


FIG. 15.—As in Fig. 8

the LMT model was constructed. PSR 1745–24 with $R \approx 1.5$ kpc is nearest to the Galactic center, followed by PSR 1800–21 with $R \approx 3.7$ kpc. The *minimum* galactocentric radii for the remaining pulsars lie between 4 and 6 kpc, but since most distances are only known with broad limits, their *true* galactocentric radii could be larger.

The values of $\langle n_e \rangle$ from Tables 3 and 4 for these 18 pulsars are displayed as a function of longitude in Figure 16a. We assume that the distribution of electrons in the inner Galaxy has axial symmetry, so that data from the first and fourth Galactic quadrants have been folded together on the same horizontal axis. Inspection of Figure 16a reveals interesting factors about the distribution of $\langle n_e \rangle$ in the inner Galaxy. The dashed line at $\langle n_e \rangle = 0.025 \text{ cm}^{-3}$ is from Weisberg et al. (1980) and represents the average mean electron density in the Galactic plane within several kpc of the Sun. One can see easily that the values of $\langle n_e \rangle$ in the inner Galaxy are not representative of

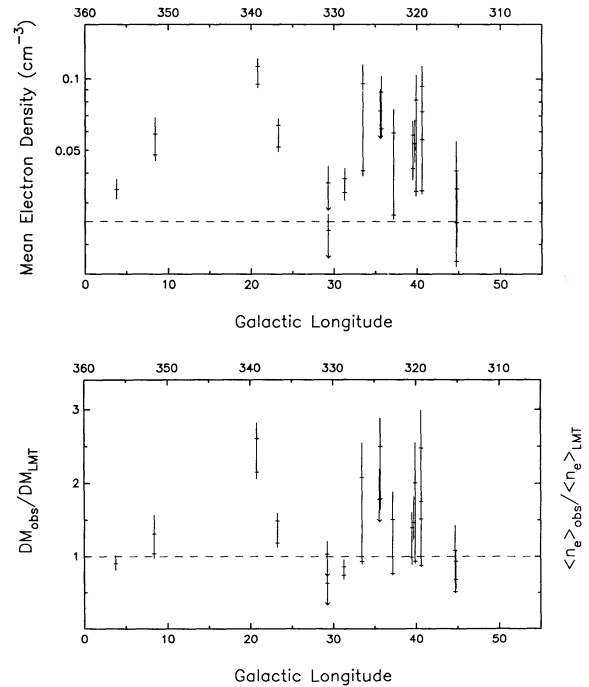


FIG. 16.—(a) Mean electron density as a function of Galactic longitude for the 18 pulsar lines of sight in the inner Galaxy (defined by $|l| \leq 45^\circ$, $|b| \leq 2^\circ$, and $DM \geq 100 \text{ pc cm}^{-3}$) toward which direct measurements of $\langle n_e \rangle$ have been made. First and fourth galactic quadrants have been folded together in the horizontal axis. The average $\langle n_e \rangle$ within a few kiloparsecs of the Sun is 0.025 cm^{-3} . Electron densities denoted by the horizontal ticks are calculated for D_L and/or D_U . Values outside this are either error estimates (*vertical lines*) or limits (*arrows*). (b) Comparison between dispersion measures calculated from the LMT model (DM_{LMT}) and the observed values (DM_{obs}) as a function of Galactic longitude for the same lines of sight as in (a). If the model and observations were in agreement, then the points would scatter about the bottom dashed line.

the local average and that $\langle n_e \rangle$ must rise in the inner Galaxy. Ables & Manchester (1976) were the first to note this enhancement of $\langle n_e \rangle$ at low $|l|$, but they had a much smaller sample size. With our increased sample size we see some evidence for a plateau of increased $\langle n_e \rangle$ on top of which there rests a peak near $|l| = 37^\circ$ with a width of 10° . A possible explanation for this behavior would be the existence of an electron density torus in addition to a more general monotonic density relation

TABLE 4
ADDITIONAL INNER GALAXY PULSARS

Pulsar (1)	l (2)	b (3)	DM (pc cm^{-3}) (4)	D_L (kpc) (5)	D_U (kpc) (6)	Electron Density (cm^{-3}) (7)
1509–58.....	320.3	–1.2	235 ± 25	4.4 ± 0.9^a	...	$\langle n_e \rangle = 0.053$
1557–50.....	330.7	1.6	270 ± 30	7.4 ± 1.1	...	$\langle n_e \rangle \leq 0.036$
1558–50.....	330.7	1.3	169.5	7.4 ± 1.1	...	$\langle n_e \rangle \leq 0.023$
1745–24.....	3.8	1.7	242.0	7.1 ± 0.7^a	...	$\langle n_e \rangle = 0.034$
1845–01.....	31.3	0.0	159.1	4.2 ± 0.4	4.8 ± 0.4	$0.033 \leq \langle n_e \rangle \leq 0.038$
1849+00.....	33.5	0.0	680 ± 60	7.1 ± 1.2	16.6 ± 0.9	$0.041 \leq \langle n_e \rangle \leq 0.096$
1855+02.....	35.6	–0.4	506	6.9 ± 1.3	...	$\langle n_e \rangle \leq 0.073$
1859+03.....	37.2	–0.6	402.9	6.8 ± 1.4	15.1 ± 0.7	$0.027 \leq \langle n_e \rangle \leq 0.059$
1859+07.....	40.6	1.1	261	2.8 ± 0.5	4.7 ± 0.8	$0.056 \leq \langle n_e \rangle \leq 0.093$
1900+01.....	35.7	–2.0	246.4	2.8 ± 0.4	4.0 ± 0.4	$0.062 \leq \langle n_e \rangle \leq 0.088$
1904+06.....	40.6	–0.3	473	6.5 ± 1.5	14.0 ± 0.5	$0.034 \leq \langle n_e \rangle \leq 0.073$
1907+10.....	44.8	1.0	148.4	4.3 ± 0.6	6.0 ± 1.6	$0.025 \leq \langle n_e \rangle \leq 0.035$

^a True distance, not a lower limit.

increasing at low R . However, we caution against over interpreting Figure 16a. The region around $l = 37^\circ$ is readily accessible to the large telescopes in the northern hemisphere, resulting in a concentration of 21 cm absorption observations. It is possible that the fluctuation in $\langle n_e \rangle$ merely reflects the clumpy distribution of the interstellar electrons, and that any well-sampled region at lower $|l|$ would give a similar result.

These new measurements of $\langle n_e \rangle$ can also be used to check the validity of the LMT model at low galactocentric radii. For each of the 18 pulsars in the inner Galaxy, a model-dependent DM was calculated by integrating the LMT model (eq. [2]) up to the distances specified in Table 3 or Table 4. A value of $R_o = 8.5$ kpc was used in this case, but the choice of R_o does not seriously affect the results. The ratio of the observed DM divided by the LMT model DM is plotted as a function of longitude in Figure 16b.

In the LMT model the electron density increases by a factor of 2 from the Sun to the Galactic center. If the LMT model accurately represents the electron density in the inner Galaxy, then all points in Figure 16b should lie along the dashed line representing $DM_{\text{obs}}/DM_{\text{LMT}} \equiv 1$. Clearly, however, the great majority of the points lie well above this line, indicating that the radial distribution of the electron density in the inner Galaxy is steeper than the LMT model term. The effect is most clearly evident in the longitude range $30^\circ \leq |l| \leq 40^\circ$, which is also the best-sampled region. Elsewhere most points are not far from unity and in some cases even lie below unity. To obtain better agreement with the observed DMs we suggest that the LMT model density should rise to 3 times the local density at the Galactic center, rather than the current twofold increase. The most discrepant point in Figure 16b at $|l| = 20^\circ$ is PSR 1641–45. Its large $\langle n_e \rangle$ ($\approx 0.1 \text{ cm}^{-3}$) is apparently anomalous, for it is one of the few pulsars toward which recombination line emission has been detected (Manchester & Mebold 1977) between us and the pulsar (i.e. at -43 km s^{-1}). Since its DM likely has a substantial contribution from a discrete source, the poor agreement with the LMT model is not surprising.

The large error bars in Figures 16a and 16b are due to the wide pulsar distance limits. This is caused by the failure of the kinematic method to tightly constrain the distance to the high-DM pulsars in the inner Galaxy. Despite this limitation, these same pulsars set a very reliable constraint on the *maximum* electron density at low R . This is because the lower distance limit and therefore the upper limit to $\langle n_e \rangle$ for these high-DM pulsars are based on the detection of H I absorption out to the tangent point. For pure circular rotation this is a geometrically defined point which is independent of the choice of a rotation curve ($D \equiv R_o \cos l$). The results rule out any *dramatic* rise, and the actual density in the inner regions of the Galaxy is surely not more than a factor of 2 higher than given by the LMT model.

4.1.2. A Simple Step Function Model

By definition $\langle n_e \rangle$ from equation (1) is a line-of-sight average and therefore does not directly give the quantity of interest \bar{n}_e , the density of the ionized gas at any point throughout the Galaxy. The goal of any proper modeling analysis would be to distinguish from the family of possible models that which best describes the electron density distribution. However, the large distance uncertainties and the relatively small number of lines of sight limit our ability to do this type of modeling. In the end, we believe the best way to derive the radial distribution of n_e will be through a statistical analysis of the newly discovered

high-DM pulsars of Johnston (1990) and Clifton & Lyne (1986), constraining the analysis with the $\langle n_e \rangle$ measurements presented here. Here we are merely interested in deriving an estimate for the *magnitude* of the rise of n_e at low R , and so we pick a simple step-function model with a decrease of $n_e(R)$ at $R \geq R_{\text{step}}$. More detailed modeling of these and other data has recently been done by Cordes et al. (1991).

In our model the electron density is equal to n_{eo} everywhere except within the boundaries of a disk of radius R_{step} where it is n_{ei} . Along a particular path, the mean electron density $\langle n_e \rangle$ is given by,

$$\langle n_e \rangle = n_{eo}(1 - p) + n_{ei}p, \quad (3)$$

where p is the fraction of the total distance that the line of sight traverses the disk. We ignore any z -dependence since we have chosen our sample of pulsars to be close to the plane $|b| \leq 2^\circ$. We use $n_{eo} = 0.025 \text{ cm}^{-3}$, determined by Weisberg et al. (1980) as the *local* mean electron density in the plane. The value for R_{step} was chosen to be 7 kpc. Only lines of sight with $|l| \leq 55^\circ$ will penetrate this disk, and outside this region there is no evidence for a larger than average $\langle n_e \rangle$, except for the anomalous Gum nebula region. The chosen value for R_{step} also marks the outer radius of the “molecular ring” (Scoville & Sanders 1987), within which it is reasonable to expect that the electron density could increase. Lowering R_{step} has the effect of decreasing p and increasing n_{ei} .

Values of n_{ei} were calculated for the 18 “inner Galaxy” pulsars in Tables 3 and 4. Pulsars with both lower and upper distances give separate estimates for n_{ei} . Although the distance uncertainties introduce wide scatter, we find the average value of n_{ei} to be 0.08 cm^{-3} . As a rough approximation the average mean electron density in the inner Galaxy is 0.08 cm^{-3} , slightly more than 3 times the local value of 0.025 cm^{-3} . There is little evidence for average electron densities in excess of 0.15 cm^{-3} . At $R = 5$ kpc (the minimum radius for the majority of our 18 pulsars) the average density for the LMT model is 0.05 cm^{-3} . Our newly adopted value of 0.08 cm^{-3} is 50% above this and confirms our earlier conclusion that the radial term in the LMT model is not steep enough in the inner Galaxy.

It is known that the neutral component of the atomic phase has a constant mass surface density of approximately $8 M_\odot \text{ pc}^{-2}$ from $R = 4$ kpc to $R = 20$ kpc (Kulkarni & Heiles 1987). Locally 20% of the atomic gas (neutral and ionized) is in the WIM (i.e., $2 M_\odot \text{ pc}^{-2}$), giving a *total* mass surface density for the atomic phase of $10 M_\odot \text{ pc}^{-2}$ (Reynolds 1989b). Scaling by the ratio of the measured electron densities ($0.08/0.025$) and assuming that the scale height of the WIM is independent of radius, one derives a mass surface density for the WIM in the inner Galaxy of $6 M_\odot \text{ pc}^{-2}$. This result is only preliminary since the scale height of the WIM in the inner Galaxy is unknown, but it suggests that at low galactocentric radii half the atomic gas is in ionized form.

4.2. The Source of the Ionization in the WIM

The WIM is the most energetically important phase of the ISM and an essential component in disk-halo interactions (Cox 1989). One of the key unanswered questions about the WIM concerns the source of the ionization. The enormous power requirements of the WIM place stringent constraints on a potential ionizing agent. Supernovae, X-rays, and cosmic rays have been suggested as potential candidates, as have UV continuum sources such as early-type stars, the nuclei of planetary nebulae and white dwarfs (Reynolds 1984).

All but two of these sources, supernovae (SNs) and O stars, fall short of maintaining the necessary heating to balance the energy loss expected from a theoretical cooling curve for the WIM (Reynolds 1990a). A further *observational* constraint on the power requirements of the WIM is given by Reynolds's (1984) measurement of the average hydrogen recombination rate α within about 2 kpc of the Sun ($\alpha = 4 \times 10^6 \text{ s}^{-1} \text{ cm}^{-2}$). Here too, it is only SNs and O stars that are able to provide this level of ionization in steady state.

On closer examination SNs also appear to be ineffective. It would require that nearly 100% of all SNs energy go into ionizing the ambient gas, whereas a much smaller fraction is expected (Abbott 1982). The constancy of the observed $[\text{S II}]/\text{H}\alpha$ ratio (≈ 0.5) in our own galaxy and other spirals such as M31 and NGC 891 presents an additional problem (Walterbos 1990, personal communication; Rand, Kulkarni, & Hester 1990; Dettmar 1990; Reynolds 1988). To reproduce the observed $[\text{S II}]/\text{H}\alpha$ ratio with a shock ionization model would require such fine tuning of the shock velocities ($60\text{--}80 \text{ km s}^{-1}$) as to make any model appear highly contrived (Rand et al. 1990).

Independent measurements of Σ^* , the average ionizing flux in the plane of the Galaxy, show that locally O stars have more than 7 times the required ionizing flux to heat the WIM (Mathis 1986; Reynolds 1984). Abbott (1982) has added up all the UV flux from O stars within 3 kpc of the Sun and finds $\Sigma^* = 31 \times 10^6 \text{ s}^{-1} \text{ cm}^{-2}$. Mezger (1978) derives $36 \times 10^6 \text{ s}^{-1} \text{ cm}^{-2}$ from the diffuse radio emission at 5 GHz between $R = 10 \text{ kpc}$ and $R = 11 \text{ kpc}$ (for $R_0 = 10 \text{ kpc}$). Moreover, the observed $[\text{S II}]/\text{H}\alpha$ ratio lies within the range of values predicted by Mathis (1986) for a diffuse photoionization model for the WIM.

However, not all of this flux is available for ionizing the diffuse medium. A large fraction of O stars are located in dense environments where their ionizing photons are "locked up" in discrete, radiation-bounded H II regions (Kulkarni & Heiles 1988). From the work of Wood & Churchwell (1989) and Leisawitz & Hauser (1988) we know that O stars spend only a small fraction (10%–20%) of their lifetimes embedded in the dense molecular clouds from which they originate. The remaining time is divided equally between being located near the molecular cloud ("blister phase") or far away from the parent cloud ("naked phase"). In the blister phase O stars form an ionization-bounded region of a few cm^{-3} . It is the naked phase portion of this evolutionary picture that is of interest here. During the naked phase the O star has moved into the diffuse ISM and is able to ionize gas and heat dust over a large volume (Cox & Mezger 1989).

There is some observational support for the existence of a naked phase. Cruz-González et al. (1974) found that on average 47% of O stars have no detectable H II regions on the Palomar Sky Survey plates. Similarly, Lynds (1980) estimates that 43% of all O stars are located *outside* bright H II regions. The percentage varies with spectral type, increasing for the later types. Bregman & Harrington (1986) used Lynds's relation along with Panagia's (1973) values for the Lyman continuum photon flux expected from early-type stars, to calculate the ionization rate in the WIM expected from O stars. Their derived ionization rate β is $8.9 \times 10^6 \text{ s}^{-1} \text{ cm}^{-2}$; within a factor of 2 of the Reynolds's (1984) estimate for the hydrogen recombination rate $\alpha = 4 \times 10^6 \text{ s}^{-1} \text{ cm}^{-2}$. Elmergreen (1976) points out that extinction by dust of faint H II regions would tend to lower the percentage estimates of Lynds (1980) and Cruz-

González et al. (1974), but this would only drive the agreement between α and β even closer. The close agreement that we have shown to exist between these two independently derived rates provides strong supportive evidence that O stars are the principal ionizing agent of the WIM.

A crucial test of the O star hypothesis was suggested by Heiles (1987a). He argued that if O stars are the primary source of ionization, then it would be expected that the density of free electrons will be traced by the distribution of O stars. Between 3.5 and 7 kpc from the Galactic center the number density of H II regions and molecular clouds peaks sharply (Scoville & Sanders 1987). This implies a high rate of star formation and hence an increased number of O stars. The observations presented here and in Paper I enable us to measure the electron density at small galactocentric radii along many lines of sight. The data presented in § 4.1 do show a clear rise in the electron density in the inner Galaxy, to about 3 times the local average. However, it remains to be shown whether the magnitude of the observed rise in the electron density is commensurate with the expected increase in the Lyman continuum flux.

We take a simple approach to this problem, recognizing that there exist a number of uncertainties. A direct determination of Σ^* from an integration of the O star luminosity function is not possible in the inner Galaxy because of dust obscuration. We must instead resort to indirect means. Mezger (1978) has used the free-free radio emission at 5 GHz as a tracer to calculate the total Lyman continuum photon flux as a function of galactocentric radius. Locally he derives $\Sigma^* = 36 \times 10^6 \text{ s}^{-1} \text{ cm}^{-2}$ and for the inner molecular ring region $\Sigma^* = 158 \times 10^6 \text{ s}^{-1} \text{ cm}^{-2}$. This estimate, while necessarily crude, shows that the ionizing flux from O stars increases by a factor of 4 from its local value to that in the ring. This increase is close to the observed threefold increase in the electron density at small galactocentric radii, and hence we conclude that our results are consistent with the hypothesis that early-type stars are the dominant ionization source for the ISM in the inner Galaxy.

There are several uncertainties and unanswered questions that remain. The measurements of the electron density are line-of-sight averages, which were converted to volume averages via a simple model. Both of these values are sensitive to the functional dependence of the filling factor ($ff \equiv \langle n_e \rangle / n_e$). In the extreme view a rising $\langle n_e \rangle$ in the inner Galaxy could be the result of an increasing filling factor for the WIM. Similarly, one could argue that the fraction ϵ of Σ^* required to heat the WIM cloud change in the inner Galaxy from its local value of approximately 15%. While we cannot rule out any radial dependence in these quantities, we find no compelling reasons to expect large changes in either ff or ϵ .

Many authors have commented on the difficulty that O stars will have in ionizing a diffuse, widespread medium. Elmergreen (1976) showed that the UV flux from O stars will ionize and evaporate neutral cloud material creating an ionization-bounded H II region where one might not have previously existed (i.e., the naked phase). In order to ionize large regions hundreds of parsecs away from an O star, Mathis (1986) claims that there will have to exist directions for which there are neutral column densities lower than 10^{17} cm^{-2} . At higher latitudes sufficient amounts of UV flux may "leak" out of the disk to provide the required level of ionization (Bregman & Harrington 1986) or runaway O stars could play an important role (Kulkarni & Heiles 1988), but recent upper limits on the H α intensity from high-velocity clouds suggest that their role has been overestimated, at least in the halo (Songaila, Bryant, &

Cowie 1989). A common thread that runs through all of the objections raised regarding the O-star hypothesis is the topology of the ISM. We simply do not know how the atomic phases of the ISM are distributed, what structures they assume, or the interrelation between them (Reynolds 1990b; Heiles 1987b). While we have used arguments based on *energetics*, that O stars are the principal heating agent of the WIM, the question of morphology remains as a potential problem and needs to be better addressed. The resolution of this problem requires more realistic modeling of the ISM and further observations of the atomic phases in our own galaxy as well as external galaxies.

5. CONCLUSIONS

Observations of 21 cm absorption toward high-dispersion measure, low-latitude pulsars have yielded measurements of the mean electron density in the inner Galaxy. Applying a simple disk model to these data we find that the electron density in the WIM rises from its local value of 0.025 cm^{-3} to approximately 0.08 cm^{-3} in the inner Galaxy. This threefold increase suggests that the warm ionized medium is a more significant fraction of the atomic gas at low R than has previously been assumed. Locally the WIM is approximately 20% of the total surface density of atomic material, but this could rise to 50% in the inner Galaxy if the scale height of the WIM is equal to its local value (i.e., 1000 pc).

There are now several arguments that can be made in support of the hypothesis that O stars are the principal heating agents of the WIM. From the list of known candidates only O stars are able to provide the level of ionization that is required. The agreement between the observed recombination rate α and the value estimated for the ionization rate from O stars in the WIM ($\beta \equiv \epsilon \Sigma^*$) is another important part of this argument. It demonstrates that a large fraction ($\epsilon \approx 15\%$) of the total UV

flux from O stars is able to escape into the diffuse component of the ISM and therefore could provide the level of ionization that is required. A rise in the electron density at low R was a key prediction of the O-star hypothesis. We have shown that n_e increases proportionally with the increased Lyman continuum flux Σ^* in the inner Galaxy. Finally, the values of the observed line ratios such as $[\text{S II}]/\text{H}\alpha$ are within the limits predicted by photoionization models of the WIM. Shock ionization could be operating at some level, but the optical line ratios suggest that its role in heating the WIM is a minor one. Problems with this picture still exist, primarily having to do with the uncertain topology of the ISM.

D. A. F. thanks Shri Kulkarni for an early push in the right direction and Ernie Seaquist for his advice and guidance along the way. T. H. H. thanks the Intel Corporation and Analog Devices Corporation for providing systems and components used for the pulsar signal averager, and Peter Miller and Earle Horton for much of the hardware and software development of the system. We thank Barry Clark for ample test time at the VLA and Ken Sowinski and other VLA staff members for extensive help in getting the spectral line gating system working. We also thank Rachel Pildis for assistance with the Arecibo observations. We thank Ron Maddelena for getting the 140 ft emission spectra for us. D. A. F. acknowledges the financial support of the Natural Sciences and Engineering Research Council of Canada through an NSERC Postdoctoral Fellowship, the National Radio Astronomy Observatory through a Jansky Postdoctoral Fellowship, and the Reinhardt Fund at the University of Toronto. J. M. C. received support under grant AST 8520530 from the National Sciences Foundation and from the National Astronomy and Ionosphere Center. J. M. W. was partially supported by NSF grants AST 8701979 and AST 8919061.

REFERENCES

- Abbott, D. C. 1982, *ApJ*, 263, 723
 Ables, J. G., & Manchester, R. N. 1976, *A&A*, 50, 177
 Altenoff, W. J., Downes, D., Pauls, T., & Schraml, J. 1979, *A&AS*, 35, 23
 Blitz, L., Fich, M., & Stark, A. A. 1982, *ApJS*, 49, 183
 Booth, R. S., & Lyne, A. G. 1976, *MNRAS*, 174, 53P
 Bregman, J. N., & Harrington, J. P. 1986, *ApJ*, 309, 833
 Burton, W. B. 1985, *A&AS*, 62, 365
 Caswell, J. L., Murry, J. D., Roger, R. S., Cole, D. J., & Cooke, D. J. 1975, *A&A*, 45, 239
 Clifton, T. R., Frail, D. A., Kulkarni, S. R., & Weisberg, J. M. 1988, *ApJ*, 333, 332 (Paper I)
 Clifton, T. R., & Lyne, A. G. 1986, *Nature*, 320, 43
 Colgran, S. W. J., Salpeter, E. E., & Terzian, Y. 1988, *ApJ*, 328, 275
 Cordes, J. M. 1986, *ApJ*, 311, 183
 Cordes, J. M., Weisberg, J. M., Frail, D. A., Spangler, S. R., & Ryan, M. 1991, *Nature*, submitted
 Cox, D. P. 1989, in *IAU Coll. 120, Structure and Dynamics of the Interstellar Medium*, ed. G. Tenorio-Tagle, M. Moles, & J. Melnick (New York: Springer), 500
 Cox, P., & Mezger, P. G. 1989, *A&AR*, 1, 49
 Crovisier, J., & Dickey, J. M. 1983, *A&A*, 122, 282
 Cruz-González, C., Recillas-Cruz, E., Costero, R., Peimbert, M., & Torres-Peimbert, S. 1974, *Rev. Mexicana Astr. Af.*, 1, 211
 Damour, T., & Taylor, J. H. 1991, *ApJ*, 366, 501
 Dettmar, R. 1990, *A&A*, 232, L15
 Diamond, P. J., Goss, W. M., Romney, J. D., Booth, R. S., Kalberla, P. M. W., & Mebold, U. 1989, *ApJ*, 347, 302
 del Romero, A., & Gómez-González, J. 1981, *A&A*, 104, 83
 Dickey, J. M., & Benson, J. M. 1982, *AJ*, 87, 278
 Dickey, J. M., Kulkarni, S. R., van Gorkom, J. H., & Heiles, C. E. 1983, *ApJS*, 53, 591
 Elmergreen, B. G. 1976, *ApJ*, 205, 405
 Fich, M., Blitz, L., & Stark, A. A. 1989, *ApJ*, 342, 272
 Frail, D. A. 1989, Ph.D. thesis, Univ. of Toronto
 Frail, D. A., & Weisberg, J. M. 1990, *AJ*, 100, 743
 Garwood, R. W., & Dickey, J. M. 1989, *ApJ*, 338, 841
 Gathier, R., Pottasch, S. R., & Goss, W. M. 1986, *A&A*, 157, 191
 Gerasimenko, T. P. 1983, *Soviet Astr. Letters*, 9, 373
 Gómez-González, J., & Guélin, M. 1974, *A&A*, 32, 441
 Gordon, C. P., Gordon, K. J., & Shalloway, A. M. 1969, *Nature*, 222, 129
 Gordon, K. J., & Gordon, C. P. 1973, *A&A*, 27, 119
 Harding, D. S., & Harding, A. K. 1982, *ApJ*, 257, 603
 Heiles, C. 1987a, in *Proc. Arecibo Upgrading Workshop*, ed. J. H. Taylor & M. M. Davis (Arecibo: NAIC), 145
 ———. 1987b, *ApJ*, 315, 555
 Johnston, S. 1990, Ph.D. thesis, Univ. of Manchester
 Kalberla, P. M. W., Goss, W. M., & Wilson, T. L. 1982, *A&A*, 106, 167
 Kassim, N. E., & Weiler, K. W. 1990, *Nature*, 343, 146
 Kovalenko, A. V. 1989, *Soviet Astr. Letters*, 15, 144
 Kulkarni, S. R., & Heiles, C. 1987, in *Interstellar Processes*, ed. D. J. Hollenbach & H. A. Thronson, Jr. (Dordrecht: Reidel), 87
 ———. 1988, in *Galactic and Extragalactic Radio Astronomy*, ed. G. L. Verschuur & K. I. Kellerman (New York: Springer), 95
 Leisawitz, D., & Hauser, M. G. 1988, *ApJ*, 332, 954
 Lockman, F. J. 1989, *ApJS*, 71, 469
 Lynds, B. T. 1980, *AJ*, 85, 1046
 Lyne, A. G., et al. 1990, *Nature*, 347, 650
 Lyne, A. G., Manchester, R. N., & Taylor, J. H. 1985, *MNRAS*, 213, 613
 Manchester, R. N., & Mebold, U. 1977, *A&A*, 59, 401
 Mathis, J. S. 1986, *ApJ*, 301, 423
 McKee, C. F., & Ostriker, J. P. 1977, *ApJ*, 218, 148
 Mezger, P. G. 1978, *A&A*, 70, 565
 Panagia, N. 1973, *AJ*, 78, 929
 Rand, R. J., Kulkarni, S. R., & Hester, J. 1990, *ApJ*, 352, L1
 Reich, W., Fürst, E., Reich, P., Sofue, Y., & Handa, T. 1986, *A&A*, 155, 185
 Reynolds, R. J. 1984, *ApJ*, 282, 191
 ———. 1988, *ApJ*, 333, 341
 Reynolds, R. J. 1989a, in *IAU Symp. 139, Galactic and Extragalactic Background Radiation*, ed. S. Bowyer & C. Leinert (Dordrecht: Reidel), 157
 ———. 1989b, *ApJ*, 339, L29
 ———. 1990a, *ApJ*, 349, L17
 ———. 1990b, *ApJ*, 348, 153

- Roberts, W. W. 1972, ApJ, 173, 259
Routledge, D., & Vaneldik, J. F. 1988, ApJ, 326, 751
Schmidt, M. 1965, in Stars and Stellar Systems, Vol. 5, ed. A Blaauw & M. Schmidt (Chicago: Univ. of Chicago Press), 513
Scoville, N. Z., & Sanders, D. B. 1987, in Interstellar Processes, ed. D. J. Hollenbach & H. A. Thronson, Jr. (Dordrecht: Reidel), 21
Silvergate, P., & Terzian, Y. 1978, AJ, 83, 1412
Songaila, A., Bryant, W., & Cowie, L. L. 1989, ApJ, 345, L71
Vivekanand, M., & Narayan, R. 1982, J. Ap. Astr., 3, 399
Weaver, H. F., & Williams, D. R. W. 1974, A&AS, 17, 1
Weisberg, J. M., Rankin, J., & Boriakoff, V. 1980, A&A, 88, 84
———. 1987, A&A, 186, 307
Wood, D. O. S., & Churchwell, E. 1989, ApJ, 340, 265